Chinese Chemical Letters 31 (2020) 1114–1118

Contents lists available at ScienceDirect

Chinese Chemical Letters

journal homepage: www.elsevier.com/locate/cclet

Communication

A WO_3-$CuWO_4$ nanostructured heterojunction for enhanced *n*-butanol sensing performance

Fanpeng Duanmu[a], Zhurui Shen[a,*], Qian Liu[a], Shuhui Zhong[b,*], Huiming Ji[a,*]

[a] *Key Laboratory of Advanced Ceramics and Machining Technology (Ministry of Education), School of Materials Science and Engineering, Tianjin University, Tianjin 300350, China*

[b] *School of Mathematics, Tianjin University, Tianjin 300350, China*

ARTICLE INFO

Article history:
Received 15 June 2019
Received in revised form 7 July 2019
Accepted 12 July 2019
Available online 13 July 2019

Keywords:
Gas sensor
Tungsten oxide
Copper tungstate
Nanostructured heterojunction
Nanoparticle
n-Butanol

ABSTRACT

Herein, a WO_3-$CuWO_4$ nanostructured heterojunction was prepared by a facile two-step hydrothermal method. It is composed of a WO_3 square microplate and $CuWO_4$ nanoparticles. Then, the gas sensing properties were investigated under optimal operating temperature (120 °C). The WO_3-$CuWO_4$ heterostructure shows good sensing performance towards *n*-butanol, with a response value up to 9.4 to towards 30 ppm *n*-butanol, and the response value is about 3 times higher than that of pristine WO_3. Its detection limit for *n*-butanol is 0.1 ppm, which indicates a potential application in lower concentration detection. Moreover, the response time of WO_3-$CuWO_4$ nanostructured heterojunction and the pristine WO_3 are 21 s and 240 s respectively, revealing that there is a faster gas sensing process in the heterostructure. A possible sensing mechanism was then proposed on the basis of experimental data and band structure analysis. The significant enhancement of WO_3-$CuWO_4$ heterostructure could be attributed to the formation of heterojunction, which brings electronic sensitization and electron transport pathway modulation. The work offered a kind of novel and cost-effective sensing materials, and inspired more novel devices based on nanostructured heterojunction mechanism.

The research on gas sensing is of great significance in many fields including household environmental safety, industrial production security and respiratory test [1–5]. Semiconductor metal oxides (SMOs) have attracted considerable attention because of their low cost, high sensitivity and good stability [6–9]. Compared with the existing gas detection technology such as gas chromatography and mass spectrometry (GC–MS), proton-transfer reaction mass spectrometry (PTR-MS), optical sensor and so on, a SMOs-based chemoresistive sensor is very promising for gas sensing because of its potential in real-time analysis, simple operating principle, facile device manufacture and ready miniaturization (Table S1 in Supporting information) [10,11]. Tungsten oxide (WO_3), a kind of n-type semiconductor whose band gap is about 2.7 eV, is one of the most well-known semiconductor gas sensing materials because of its high chemical stability and environmental non-toxicity [12–15]. However, the practical application of pure WO_3 in gas sensing has suffered from its high operating temperature, low selectivity and high detection limit. Combining the WO_3 with other compounds (mostly metal oxides) is an effective way to enhance the gas sensing performance, which has been reported to be applied in detecting H_2, NH_3, NO_x [16–18], while there are few reports focusing on the detection of volatile organic compounds (VOCs). VOCs, widely existing in our inhabited environment, refer to the organic molecules that exist in the form of gas at room temperature, which usually do harm to environment and human health [19–21]. For instance, *n*-butanol, a kind of industrial intermediate chemical, is explosive, flammable and slightly toxic [7,22,23]. Therefore, it is necessary to monitor the VOCs indoor and outdoor in order to protect air quality and environment safety.

Herein, WO_3 crystallized microplates modified with $CuWO_4$ nanoparticles were synthesized in this study using a facile two-step hydrothermal method. The morphology, phase constitute and surface chemical state are discussed in details. The gas sensing reaction process, performance and mechanism towards *n*-butanol are studied. Notably, it is found that the $CuWO_4$-modified WO_3 microplates have quite low operating temperature (120 °C) and short response time (21 s), and its response to 30 ppm *n*-butanol reaches 9.4, which indicate a remarkable enhancement of gas sensing performance, contributed by the formation of WO_3-$CuWO_4$ nanostructured heterojunction. A possible mechanism was

* Corresponding authors.
E-mail addresses: shenzhurui@tju.edu.cn (Z. Shen), zhshuhui@tju.edu.cn (S. Zhong), jihuiming@tju.edu.cn (H. Ji).

https://doi.org/10.1016/j.cclet.2019.07.032

proposed. This work will be conducive to the further development of high-efficiency, low-toxicity, low-cost and convenient semiconductor metal oxides-based gas sensing applications.

The WO_3-$CuWO_4$ nanostructured heterojunction was prepared *via* a two-step hydrothermal process, the procedure illustration is shown in the Fig. S1 (Supporting information). First, the WO_3 microplates were prepared using a hydrothermal method as our previous work reported [24]. Briefly, $Na_2WO_4{\cdot}2H_2O$ (1.65 g) was dissolved in 30 mL DI water, and 5 mL HCl (38 wt%) was added into the solution. After magnetically stirring for 1 h, 0.45 g $H_2C_2O_4$ was added into the solution. The mixture was stirred for 1 h and transferred into a 50 mL Teflon-lined stainless steel autoclave, sealed and heated at 120 °C for 12 h. After centrifugation and washing by DI water and ethanol, the as-prepared precipitate was dried and calcined at 400 °C for 2 h. Then, to obtain the WO_3-$CuWO_4$ nanostructured heterojunction, a mixture of as-prepared WO_3 microplates (40 mg) and $Cu(NO_3)_2{\cdot}3H_2O$ (42 mg) in 20 mL deionized water was magnetically stirred at room temperature for 30 min. After that, the suspension solution was transferred to a 25 mL Teflon-lined stainless steel autoclave, sealed and heated at 120 °C for 1.5 h. The precipitate was washed with DI water and ethanol, and dried in air at 80 °C.

Fig. S2 (Supporting information) shows the schematic diagram of gas sensor device and the electric circuit of the gas sensing measurement system. Side-heating gas sensors were applied to test the gas sensing properties of WO_3 microplates and WO_3-$CuWO_4$ nanostructured heterojunction. In a typical procedure, a Ni-Cr resistance wire used as a heater was inserted into an aluminum tube equipping with two gold electrode circles and four platinum wires. The sample powder was mixed with deionized water to form a paste, which was used to make a thin film covering the aluminum tube, the film thickness is about 20 μm (Fig. S3 in Supporting information). During the measurement, a heating current (I_{heat}) was supplied to the heater. A load resistor (R_L) was connected to the sensor, whose voltage (V_L) was measured for calculating the sensor resistance through a computer connected to the testing apparatus. The gas sensing properties of our samples were measured by a CGS-8 gas sensor analysis system (Beijing Elite Tech) using a static gas distribution method as our previous report [7], and the schematic diagram of measurement system is shown in Fig. S4 (Supporting information). The sensor response is defined as the ratio (R_a/R_g) of the sensor resistance in air (R_a) and that in the text gas (R_g). The response time and recovery time are defined as the time to reach 90% of the total resistance change during the response process and the recovery process. During the measurement, the indoor relative humidity is 15%–30% and the ambient temperature is 25 °C.

The morphologies represented by scanning electron microscopy (SEM) images are shown in Fig. 1. It is found that the pure WO_3 presents a square-plate shape with the mean size of about 500 nm (Fig. 1c). By comparing Figs. 1c and d, we find that after the second hydrothermal process, the WO_3-$CuWO_4$ nanostructured heterojunction was obtained, and the sphere-like $CuWO_4$ nanoparticles grew outwards on the edges and surface of WO_3 square microplates. The crystal structures of WO_3 and WO_3-$CuWO_4$ were characterized by X-ray diffraction (XRD), where the diffraction peaks can be indexed with WO_3 standard card (JCPDS No. 83-0950) [25] as shown in Fig. 2. There were no visible changes in the XRD pattern with $CuWO_4$-loading and no peaks corresponding to $CuWO_4$ phase. It can be supposed that $CuWO_4$ nanoparticle of the WO_3-$CuWO_4$ nanostructured heterojunction has no obvious crystallinity, which is different with the pure $CuWO_4$ nanoparticle (Fig. S5 in Supporting information), which can be confirmed by the analysis of micro-morphology. Moreover, the result of Brunauer-Emmett-Teller (BET) shows that the specific surface area of WO_3-$CuWO_4$ nanostructured heterojunction is 11.4 m^2/g, which is not

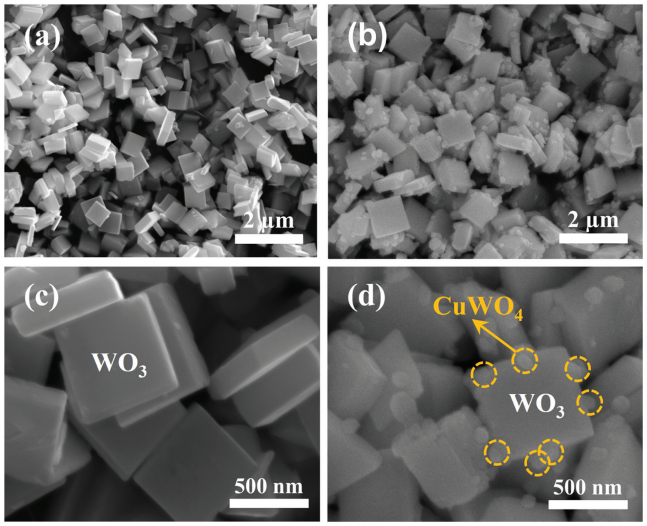

Fig. 1. SEM images of WO_3 microplates (a, c) and WO_3-$CuWO_4$ (b, d).

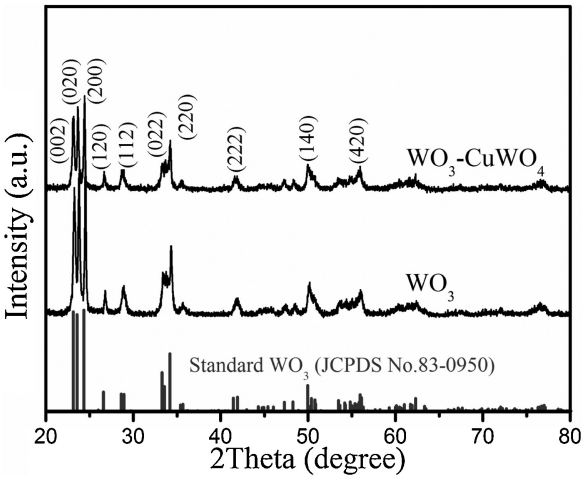

Fig. 2. XRD patterns of WO_3 microplates and WO_3-$CuWO_4$.

significantly larger than that of WO_3 microplates (6.1 m^2/g) as shown in Fig. S6 (Supporting information), and the lower specific surface area can be attributed to the larger size of microplates. Figs. 3a-c display the transmission electron microscopy (TEM) images of WO_3-$CuWO_4$. The $CuWO_4$ nanoparticles are dispersed on the edges and surface of WO_3 microplates as shown in Fig. 3a. From Figs. 3b and c, it can be seen that there is close adhesion between $CuWO_4$ nanoparticles and WO_3 microplates. Clear lattice fringes in Fig. 3c approve that these WO_3 microplates have good crystallinity, where the lattice inter-planar spacing determined to 0.365 nm corresponds to (200) plane of monoclinic WO_3 [26,27]. In contrast, Fig. 3c shows that the $CuWO_4$ nanoparticles are non-crystallized, which is consistent with the result of XRD. Meanwhile, we can find that some amorphous $CuWO_4$ layer is distributed unevenly on the surface of WO_3 microplate. In Fig. 3d, the energy-dispersive X-ray spectrometer (EDX) elemental mapping taken from a corner of one WO_3 plate loading with $CuWO_4$ particles clearly identifies the spatial distribution of W, Cu and O elements. We can find that the signals of W element not only concentrate on the square plate, but also exist in the particle area. The signals of Cu are mainly enriched in these particle area, and appear on the square plate which can be attributed to the appearance of amorphous $CuWO_4$ layer. Moreover, the signals of O present at these two areas. Considering

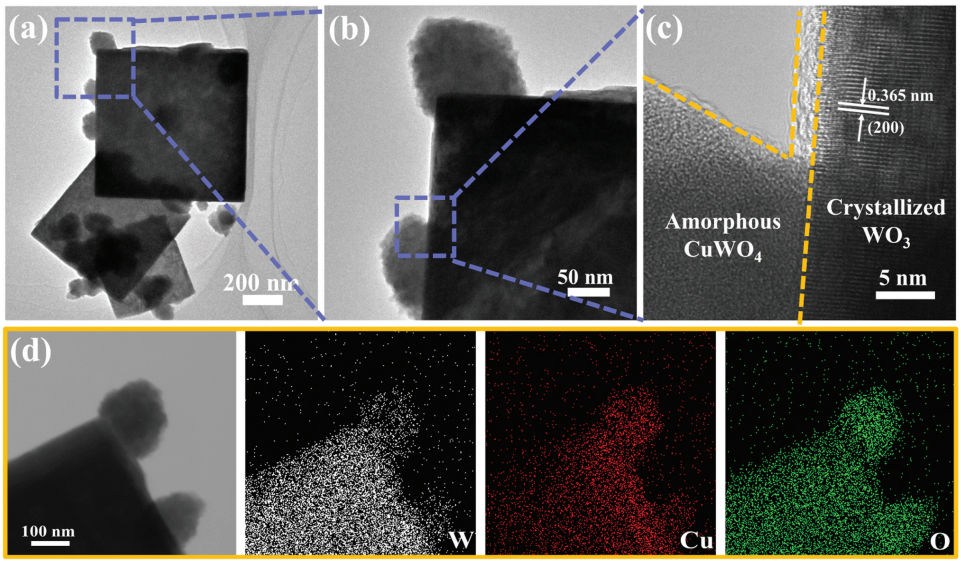

Fig. 3. HRTEM images (a, b, c) and EDS elemental mapping images (d) of W, Cu, O of WO_3-$CuWO_4$.

the results of XRD, HRTEM (high-resolution transmission electron microscopy) and EDX, the nanoparticle can be confirmed as $CuWO_4$ and the microplate can be identified as WO_3.

Herein, to understand the surface nature and chemical valence state, X-ray photoelectron spectroscopy (XPS) analysis was performed for WO_3 and WO_3-$CuWO_4$ (Fig. S7 in Supporting information). Fig. S7a shows that the W 4f spectra of WO_3 and WO_3-$CuWO_4$ were similar for their binding energy and distribution. The strong peaks at ~35.6 eV and ~37.7 eV are attributed to W^{6+} in WO_3, while the peaks of W^{6+} in WO_3-$CuWO_4$, with a little blue shift, are at ~35.8 eV and ~37.9 eV, revealing that higher oxidation state of W element in WO_3-$CuWO_4$ [28,29]. Apparently, there was no signal of Cu 2p spectra of WO_3 in Fig. S7b. Moreover, the Cu 2p spectra of WO_3-$CuWO_4$ displays a different spectral shape compared with the Cu^{2+} in CuO, with a lower satellite/main peak ($2p_{3/2}$) intensity ratio, which confirms the existence of $CuWO_4$ [30]. Fig. S7c exhibits the high resolution O 1s spectra with asymmetric shape which can be fitted by three peaks. The peaks at 530.2 eV and 530.4 eV can be regarded as typical surface lattice oxygen, while the peaks at 531.1 eV and 532.7 eV could be characterized as surface-absorbed oxygen species (*i.e.*, O^- and O^{2-}) [26,31,32]. Comparing these two O 1s spectra in Fig. S7c, it is found that the $CuWO_4$ has more surface-absorbed oxygen species, which would be beneficial to the surface gas sensing reaction [33]. Furthermore, the result of Fourier transform infrared spectrometry (FTIR) shown in Fig. S8 (Supporting information) indicates the similar surface fundamental lattice vibration of WO_3.

Fig. 4a shows the gas response of the pristine and the $CuWO_4$-functionalized WO_3 microplates, towards 30 ppm *n*-butanol at different operating temperature. It is depicted that the response value has a maximum value with the change of operating temperature. The maximum responses of WO_3 and WO_3-$CuWO_4$ sensors appear at 280 °C and 120 °C, respectively, and the optimal operating temperature of the latter is much lower than the former and other WO_3-based materials. The responses of WO_3 and WO_3-$CuWO_4$ sensors towards 10 ppm different gases were measured at 120 °C as shown in Fig. 4b, and obviously the WO_3-$CuWO_4$ shows enhanced responses to those test gases compared with WO_3 microplates especially for *n*-butanol sensing, and the corresponding transient resistance curves are shown in Fig. S9 (Supporting information). Also, the response of WO_3-$CuWO_4$ sensor to *n*-butanol is significantly higher than those to other test gases. The gas responses towards different *n*-butanol concentration varying from 0.1 ppm to 30 ppm at 120 °C are shown in Fig. 4c and the corresponding transient resistance curves are given in Fig. 4d. From the transient resistance curve of WO_3-$CuWO_4$ sensor in Fig. 4d, one can observe that the sensor resistance decreased abruptly when *n*-butanol was introduced, and increased fast when the sensor was exposed in ambient air again. The sensor response were calculated and shown in Fig. 4c, which reveals that the WO_3-$CuWO_4$ sensor has improved responses to different concentration of *n*-butanol. The response time and recovery time were calculated and noted in Figs. 4e and f. The response time of WO_3 microplates sensor and WO_3-$CuWO_4$ sensor are 240 s and 21 s, and the recovery time of these two sensors are 169 s and 116 s respectively, which reveals a faster kinetic process of gas sensing reaction on the surface of WO_3-$CuWO_4$ nanostructured heterojunction [34,35].

A possible model for the enhanced sensing performance of WO_3-$CuWO_4$ sensor is demonstrated in Fig. 5. When the $CuWO_4$ particles were loaded on the surface of WO_3 microplates, the WO_3-$CuWO_4$ heterojunction was obtained due to their energy level structure as reported in pervious literature [36,37], resulting that the electrons transfer from the WO_3 to $CuWO_4$ and that the expansion of electron depletion layer (EDL) [8]. As shown in Fig. 5a, the formation and expansion of the EDL would narrow the electron transport pathway and increase the resistance. Thus, upon exposure to *n*-butanol, the chemisorbed oxygen species participate in the surface gas reaction and release electrons to transfer into the WO_3 microplates (Figs. 5b and c), leading to the decrease of EDL thickness, which results that the WO_3-$CuWO_4$ has a larger resistance change and an enhanced response [38]. The sensing reaction process is expressed through the following Eqs. 1–4 [2,33]:

$$O_2(gas) = O_2(ads) \quad (1)$$

$$O_2(ads) + e^- = O_2^-(ads)(T < 100\ ^\circ C) \quad (2)$$

$$O_2^-(ads) + e^- = 2O^-(ads)(100\ ^\circ C < T < 300\ ^\circ C) \quad (3)$$

$$C_4H_{10}O + 12O^-(ads) = 4CO_2 + 5H_2O + 12e^- \quad (4)$$

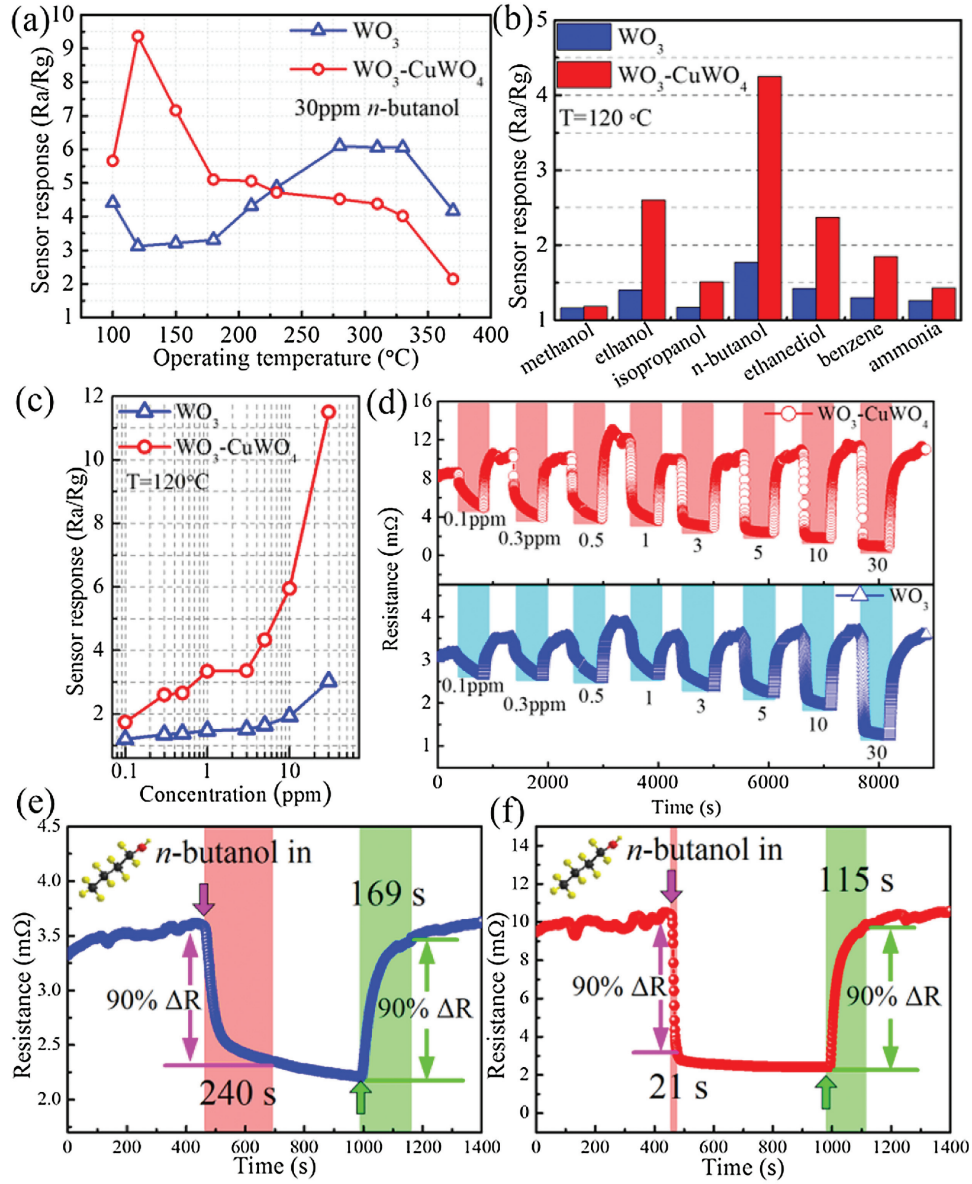

Fig. 4. (a) Sensor responses of WO_3 microplates and WO_3-$CuWO_4$ to *n*-butanol (30 ppm) as a function of operating temperature; (b) Sensor responses of WO_3 microplates and WO_3-$CuWO_4$ to 10 ppm different gases (methanol, ethanol, isopropanol, *n*-butanol, ethanediol, benzene, ammonia) at 120 °C; (c) Sensor responses and (d) transient responses to 0.1–30 ppm *n*-butanol at 120 °C; response and recovery curves of the sensors to 5 ppm *n*-butanol at 120 °C: (e) WO_3 microplates, (f) WO_3-$CuWO_4$.

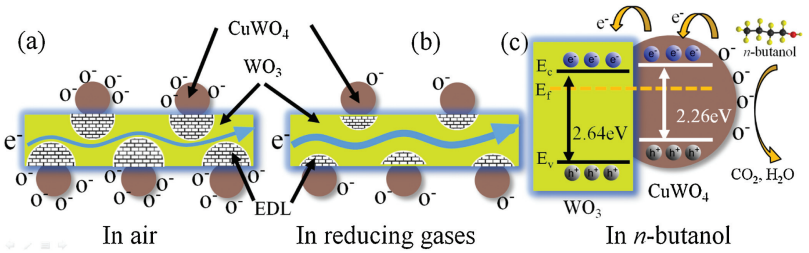

Fig. 5. Illustration of sensing mechanism of WO_3-$CuWO_4$ nanostructured heterojunction: (a) the expansion of EDL in air, (b) the decrease of EDL thickness in reducing gases, (c) the energy level structure of WO_3-$CuWO_4$ nanostructured heterojunction.

In addition to the electron transport channel modulation mentioned above, compared to the pure WO_3 microplates, the decoration of $CuWO_4$ particles promotes the chemisorption of oxygen species which was revealed by the result of XPS, and this leads to an enhancement in sensitivity of composite [20]. In summary, the fast response-recovery and high gas response to *n*-butanol of the $CuWO_4$ nanoparticles decorated bulky WO_3 microplates can be attributed to their synergetic effect as well as the heterojunction at their interface, leading to adequate surface adsorption of oxygen species and efficient electron transport [39].

In conclusion, a WO_3-$CuWO_4$ nanostructured heterojunction was manufactured through a facile two-step hydrothermal route. The morphologies of as-prepared samples investigated by SEM and TEM show that $CuWO_4$ nanoparticles are closely combined with the WO_3. Decorating WO_3 with $CuWO_4$ nanoparticles can reduce the optimum operating temperature of *n*-butanol, which decrease from 280 °C to 120 °C. The WO_3-$CuWO_4$ achieved the gas sensing selectivity to *n*-butanol at 120 °C, and the response value to 30 ppm *n*-butanol can reach 9.4. Moreover, the WO_3-$CuWO_4$ has shorter response time to 5 ppm *n*-butanol, which is only 21 s. The measured results indicate that the WO_3-$CuWO_4$ nanostructured heterojunction is a potential gas sensing material for monitoring the flammable and harmful volatile organic compounds.

Acknowledgment

We acknowledge the financially support by the National Natural Science Foundation of China as general projects (Nos. 21303118 and 21872102).

Appendix A. Supplementary data

Supplementary material related to this article can be found, in the online version, at doi:https://doi.org/10.1016/j.cclet.2019.07.032.

References

[1] J.M. Walker, S.A. Akbar, P.A. Morris, Sens. Actuators B: Chem. 286 (2019) 624–640.
[2] F. Liu, G. Huang, X. Wang, et al., Sens. Actuators B: Chem. 277 (2018) 144–151.
[3] R.D. Vries, P. Brinkman, M.P.V.D. Schee, et al., J. Breath Res. 9 (2015) 046001.
[4] X. Zhou, X. Cheng, Y. Zhu, et al., Chin. Chem. Lett. 29 (2018) 405–416.
[5] J. Ma, L. Mei, Y. Chen, et al., Nanoscale 5 (2013) 895–898.
[6] G. Korotcenkov, B.K. Cho, Sens. Actuators B: Chem. 244 (2017) 182–210.
[7] M. Wang, Z. Shen, X. Zhao, et al., J. Hazard. Mater. 371 (2019) 352–361.
[8] Q. Zhang, H. Zhang, M. Xu, et al., Chin. Chem. Lett. 29 (2018) 538–542.
[9] X. Chen, N. Deng, X. Zhang, et al., J. Nanopart. Res. 21 (2019) 77.
[10] V. Saasa, T. Malwela, M. Beukes, et al., Diagnostics 8 (2018) 12.
[11] Y.C. Hsieh, D.J. Yao, J. Micromech. Microeng. 28 (2018) 093001.
[12] Y. Zhang, D. Zhang, X. Xu, B. Zhang, Chin. Chem. Lett. 29 (2018) 1350–1354.
[13] Y. Zeng, Z. Hua, X. Tian, et al., Sens. Actuators B: Chem. 273 (2018) 1291–1299.
[14] X. Cao, X. Zang, X. Zhou, M. Chen, Y. Ding, Chin. Chem. Lett. 29 (2018) 811–814.
[15] M. Bao, Y. Chen, F. Li, et al., Nanoscale 6 (2014) 4063–4066.
[16] J. Han, T.Y. Wang, T.T. Li, et al., Adv. Mater. Interfaces 5 (2018) 1701167.
[17] F. Perrozzi, S.M. Emamjomeh, V. Paolucci, et al., Sens. Actuators B: Chem. 243 (2017) 812–822.
[18] Y. Xiong, Z. Zhu, T. Guo, H. Li, Q. Xue, J. Hazard. Mater. 353 (2018) 290–299.
[19] H. Dai, S. Jing, H. Wang, et al., Sci. Total Environ. 577 (2017) 73–83.
[20] T. Petry, E. Cazelle, P. Lloyd, R. Mascarenhas, G. Stijntjes, Environ. Sci.: Processes Impacts 15 (2013) 1369–1382.
[21] J. Zheng, M. Chang, H. Xie, P. Guo, J. Clean. Prod. 127 (2016) 249–261.
[22] Y. Chen, Z. Shen, Q. Jia, J. Zhao, et al., RSC Adv. 6 (2016) 2504–2511.
[23] A. Mirzaei, S.G. Leonardi, G. Neri, Ceram. Int. 42 (2016) 15119–15141.
[24] Q. Zhang, X.X. Qin, F.P. Duanmu, et al., Angew. Chem. Int. Ed. 57 (2018) 9351–9356.
[25] Y.Q. Rong, X.F. Yang, W.D. Zhang, Y.X. Yu, Mater. Lett. 246 (2019) 161–164.
[26] J. Fu, Q. Xu, J. Low, C. Jiang, J. Yu, Appl. Catal. B 243 (2019) 556–565.
[27] S. Xiao, B. Liu, R. Zhou, et al., Sens. Actuators B: Chem. 254 (2018) 966–972.
[28] Y. Li, K. Chang, H. Tang, et al., Electrochim. Acta 298 (2019) 640–649.
[29] R. Lei, H. Zhang, H. Ni, et al., Appl. Surf. Sci. 463 (2019) 363–373.
[30] A. Stanoiu, C.E. Simion, J.M. Calderon-Moreno, et al., J. Hazard. Mater. 331 (2017) 150–160.
[31] Y. Wang, Y. Zeng, L. Wang, et al., Sens. Actuators B: Chem. 283 (2019) 693–704.
[32] F. Chen, H. Huang, Y. Zhang, T. Zhang, Chin. Chem. Lett. 28 (2017) 2244–2250.
[33] W. Tang, J. Wang, Sens. Actuators B: Chem. 207 (2015) 66–73.
[34] G.J. Sun, S.W. Choi, A. Katoch, P. Wu, S.S. Kim, J. Mater. Chem. C: Mater. Opt. Electron. Devices 1 (2013) 5454–5462.
[35] A. Kumar, S. Samanta, A. Singh, et al., ACS Appl. Mater. Interfaces 7 (2015) 17713–17724.
[36] S.S. Kalanur, J.Y. Hwang, H. Seo, J. Catal. 350 (2017) 197–202.
[37] F. Zhan, J. Li, W. Li, et al., Int. J. Hydrogen Energy 40 (2015) 6512–6520.
[38] W. Wang, F. Liu, B. Wang, Y. Wang, Chin. Chem. Lett. 30 (2019) 1261–1265.
[39] L. Zhu, W. Zeng, Y. Li, Mater. Lett. 231 (2018) 5–7.